

η -nucleus interaction from the $d + d$ reaction around the η production threshold

N. Ikeno¹, H. Nagahiro^{2,3}, D. Jido⁴, and S. Hirezaki²

¹ Department of Life and Environmental Agricultural Sciences, Tottori University, Tottori 680-8551, Japan

² Department of Physics, Nara Women's University, Nara 630-8506, Japan

³ Research Center for Nuclear Physics (RCNP), Osaka University, Ibaraki 567-0047, Japan,

⁴ Department of Physics, Tokyo Metropolitan University, Hachioji 192-0397, Japan

Received: date / Revised version: date

Abstract. The η mesic nucleus is considered to be one of the interesting exotic many body systems and has been studied since 1980's theoretically and experimentally. Recently, the formation of the η mesic nucleus in the fusion reactions of the light nuclei such as $d + d \rightarrow (\eta + \alpha) \rightarrow X$ has been proposed and the experiments have been performed by WASA-at-COSY. We develop a theoretical model to evaluate the formation rate of the η mesic nucleus in the fusion reactions and show the calculated results. We find that the η bound states could be observed in the reactions in cases with the strong attractive and small absorptive η -nucleus interactions. We compare our results with existing data of the $d + d \rightarrow \eta + \alpha$ and the $d + d \rightarrow {}^3\text{He} + N + \pi$ reactions. We find that the analyses by our theoretical model with the existing data can provide new information on the η -nucleus interaction.

PACS. 14.40.Aq pi, K, and eta mesons – 36.10.Gv Mesonic, hyperonic and antiprotonic atoms and molecules – 25.60.Pj Fusion reactions

1 Introduction

The existence of the bound states of the η meson in nucleus (η mesic nuclei) were predicted first by Haider and Liu [1] in 1980's. Stimulated by this theoretical result, there have been many studies of the structure and the formation reactions of the η mesic nucleus [2, 3, 4, 5, 6, 7, 8, 9, 10, 11, 12, 13, 14, 15, 16, 17, 18, 19, 20, 21, 22, 23, 24]. Recently, the η -nucleon and η -nucleus interactions have been studied theoretically in the context of the chiral symmetry of the strong interaction and the η mesic nucleus can be considered as one of the interesting objects to investigate the aspects of the chiral symmetry at finite density [9, 12, 13, 14, 15, 18, 20, 23]. As for the experimental studies, the first attempt to observe the η mesic nucleus was performed by the (π^+, p) reaction with finite momentum transfer [2], and the interpretation of the data is still controversial [23]. After that, there were many experimental searches of the bound states as reported in Refs. [3, 7, 8, 16, 22] for example. The systems with η in the light nucleus such as η - ${}^3\text{He}$ state also have been studied seriously [25, 26, 27] and the data of the $p + d \rightarrow \eta + {}^3\text{He}$ reaction were studied to deduce η - ${}^3\text{He}$ interaction [28]. So far, the existence of the η -Mg bound state was concluded in Ref. [22]. However, we have not found any decisive evidence of the existence of the η bound state in lighter nuclei like He.

Recently, the new experiments of the $d + d \rightarrow (\eta + \alpha) \rightarrow X$ reaction have been proposed and performed at WASA-

at-COSY [29, 30, 31, 32, 33, 34, 35]. In the experiments, the formation cross section of the η mesic nucleus in the α particle in the $d + d$ fusion reaction is planned to be measured by observing the emitted particles from the decay of the η mesic nucleus below the η production threshold. The formation rate of the emitting particles is expected to be enhanced at the resonance energy of the η bound state formation. The shape of the observed spectra in Ref. [35] were smooth without any clear peak structures, and the upper limit of the η -nucleus formation cross section was reported to be around 3–6 nb for $d + d \rightarrow {}^3\text{He} + n + \pi^0$ reaction [35]. To evaluate these upper limits, the Fermi motion of N^* in nucleus [36] is also taken into account. The upper limit for ${}^3\text{He} + p + \pi^-$ final state is two times larger because of isospin [35]. There were also the data of η production reaction $d + d \rightarrow \eta + \alpha$ above the threshold [37, 38, 39], which are expected to provide the valuable information on the reaction mechanism.

In this paper, we develop a theoretical model to evaluate the formation cross section of the η bound states in the $d + d$ reaction and show the numerical results. This theoretical model can be used to deduce the information on the η -nucleus interaction from the experimental spectra. We explain the details of our theoretical model in section 2. We show the numerical results and compare them with the existing data in section 3 to deduce the informa-

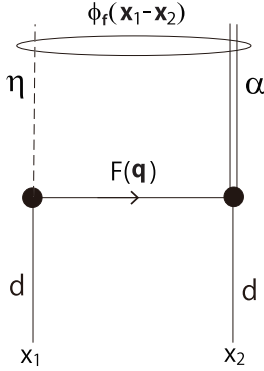


Fig. 1. The schematic diagram of the $d + d \rightarrow \eta + \alpha$ reaction.

tion on η -nucleus interaction, and summarize this paper in section 4.

2 Formulation

In this section, we consider the $d + d \rightarrow (\eta + \alpha) \rightarrow X$ reaction and explain our theoretical model developed in this article. In the experiments of this reaction at WASA-at-COSY [29, 30, 31, 32, 33, 34], the total energy of the system is varied by changing the deuteron beam momentum around the $\eta + \alpha$ threshold energy, which corresponds to the beam momentum $p = 2.3$ GeV/c, and the $\eta + \alpha$ bound state production signal is expected to be observed as peak structures of the cross section of the $d + d \rightarrow {}^3\text{He} + p + \pi^-$ and $d + d \rightarrow {}^3\text{He} + n + \pi^0$ reactions in the energy region below the η - α production threshold energy region.

Based on these considerations, we have developed a phenomenological model described below. In the model, the fusion and η meson production processes are phenomenologically parameterized and the Green's function technique is used to sum up all η - α final states.

First we formulate the transition amplitude for the $d + d \rightarrow \eta + \alpha$ reaction. We adopt the framework of the hadron reaction phenomenologically. We take a model in which the η meson production and the $d + d \rightarrow \alpha$ fusion take place in a finite size region as schematically pictured in Fig. 1. All the information on the finiteness of the reaction range, the spacial dimensions of the nuclear sizes, the structure of the deuterons and the alpha and overlap of their wavefunctions is represented by transition form factor $F(\mathbf{q})$. We are interested in the η production at the threshold, so that the final state, η and α , is dominated by s wave and, thus, the total spin-parity of the final state with a pseudo scalar (η) and a scalar (α) bosons is 0^- . Deuteron having spin 1 is represented by an axial vector boson. According to Lorentz invariance, pseudoscalar 0^- state can be made out of two axial-vectors 1^+ by so-called anomalous coupling like $\epsilon^{\mu\nu\rho\sigma} \partial_\mu A_\nu \partial_\rho A_\sigma P S$, where A_μ and P are an axial-vector boson and a pseudoscalar boson, respectively. S is a scalar boson. Thus, the interaction Hamiltonian may be written as

$$\mathcal{H}_{\text{int}} = -ic\epsilon^{ijk}((\partial_{x_2^0} \nabla_{x_1}^i - \partial_{x_1^0} \nabla_{x_2}^i) \hat{\phi}_d^j(x_1) \hat{\phi}_d^k(x_2))$$

$$\hat{\phi}_\eta^\dagger(x_1) \hat{\phi}_\alpha^\dagger(x_2) \mathcal{F}(x_1, x_2) \quad (1)$$

where $\hat{\phi}_d^i(x)$ is the deuteron field operator with spin index i , $\hat{\phi}_\eta^\dagger(x)$ and $\hat{\phi}_\alpha^\dagger(x)$ are the creation operators for η and α , respectively, and c expresses the interaction strength. The interaction strength c will be adjusted so as to reproduce the observed cross section. The function $\mathcal{F}(x_1, x_2)$ in Eq. (1) represents non-local transition form factor of $d + d \rightarrow \eta + \alpha$, which is supposed to include the information on the $d + d \rightarrow \alpha$ fusion, and the η meson production in the hadronic interaction such as $N + N \rightarrow \eta + N + N$. Assuming the translational invariance, we define the Fourier transformation

$$\mathcal{F}(x_1, x_2) = \int \frac{d^4q}{(2\pi)^4} F(\mathbf{q}) e^{iq \cdot (x_1 - x_2)}. \quad (2)$$

The momentum transfer \mathbf{q} of the reaction is large and all nucleons should participate in the fusion reaction equally. Since it is hard to calculate $F(\mathbf{q})$ in a microscopic way, we treat it phenomenologically and assume a functional form of $F(\mathbf{q})$ in the numerical evaluation.

Letting the wave functions of the incident deuterons labeled by d_1 and d_2 be given by plane waves with momentum p_1 for deuteron d_1 and p_2 for deuteron d_2 and writing the wave functions of η and α in the final state as $\phi_\eta^\dagger(\mathbf{x}) e^{-iE_\eta x^0}$ and $\phi_\alpha^\dagger(\mathbf{x}) e^{-iE_\alpha x^0}$ with the η and α energies E_η and E_α , respectively, we obtain the connected part of the S -matrix in the center of mass frame:

$$\begin{aligned} S &= -i\mathcal{N}_{d_1} \mathcal{N}_{d_2} \mathcal{N}_\eta \mathcal{N}_\alpha c \int d^4x_1 d^4x_2 \epsilon^{ijk} (\partial_{x_2^0} \nabla_{x_1}^i - \partial_{x_1^0} \nabla_{x_2}^i) \\ &\quad \left[\chi_{d_1}^j \chi_{d_2}^k e^{-ip_1 \cdot x_1} e^{-ip_2 \cdot x_2} + \chi_{d_2}^j \chi_{d_1}^k e^{-ip_2 \cdot x_1} e^{-ip_1 \cdot x_2} \right] \\ &\quad \times \int \frac{d^4q}{(2\pi)^4} F(\mathbf{q}) e^{iq \cdot (x_1 - x_2)} \phi_\eta^*(\mathbf{x}_1) e^{iE_\eta x_1^0} \phi_\alpha^*(\mathbf{x}_2) e^{iE_\alpha x_2^0} \end{aligned} \quad (3)$$

where χ_{d_1} and χ_{d_2} are the spin wave functions for deuteron d_1 and d_2 , respectively, and the normalization factors \mathcal{N}_i are given as $\mathcal{N}_i = \sqrt{M_i/E_i}$ with mass M_i and energy E_i . Operating the derivatives onto the wave functions, we have the S -matrix as

$$\begin{aligned} S &= -i2\pi\delta(E_1 + E_2 - E_f) \mathcal{N}_{d_1} \mathcal{N}_{d_2} \mathcal{N}_\eta \mathcal{N}_\alpha \\ &\quad \times c \int d\mathbf{x}_1 d\mathbf{x}_2 \epsilon^{ijk} 2(E_2 p_1^i - E_1 p_2^i) \chi_{d_1}^j \chi_{d_2}^k e^{ip_1 \cdot x_1} e^{ip_2 \cdot x_2} \\ &\quad \times \int \frac{d\mathbf{q}}{(2\pi)^3} F(\mathbf{q}) e^{-iq \cdot (x_1 - x_2)} \phi_\eta^*(\mathbf{x}_1) \phi_\alpha^*(\mathbf{x}_2), \end{aligned} \quad (4)$$

where E_1 and E_2 are the energies for deuteron d_1 and d_2 , respectively, $E_f = E_\eta + E_\alpha$ and the integrations in terms of the time components provide energy conservation

$$\begin{aligned} &\int d x_1^0 d x_2^0 \frac{d q_0}{2\pi} e^{-i x_1^0 (E_1 - q^0 - E_\eta)} e^{-i x_2^0 (E_2 + q^0 - E_\alpha)} \\ &= 2\pi\delta(E_1 + E_2 - E_f). \end{aligned} \quad (5)$$

In order to perform the spacial integrals, we introduce the relative coordinate for the final state, \mathbf{R} and \mathbf{r} , defined

as

$$\mathbf{R} = \frac{m_\eta \mathbf{x}_1 + M_\alpha \mathbf{x}_2}{m_\eta + M_\alpha}, \quad (6)$$

$$\mathbf{r} = \mathbf{x}_1 - \mathbf{x}_2. \quad (7)$$

We also introduce the wave function for the relative motion of the final state, $\phi_f(\mathbf{r})$, and assume that the center of mass motion of the η and α system is written as the plane wave. This implies that we replace the η and α wave functions as follows:

$$\mathcal{N}_\eta \mathcal{N}_\alpha \phi_\eta(\mathbf{x}_1) \phi_\alpha(\mathbf{x}_2) \rightarrow \mathcal{N}_f e^{i\mathbf{p}_f \cdot \mathbf{R}} \phi_f(\mathbf{r}), \quad (8)$$

with the momentum of the center of motion $\mathbf{p}_f = \mathbf{p}_\eta + \mathbf{p}_\alpha$ and the normalization of the wave function of relative motion $\phi_f(\mathbf{x})$ given as $\int d\mathbf{x} |\phi_f(\mathbf{x})|^2 = 1$. In this coordinate, the S -matrix is written as

$$\begin{aligned} S &= -i2\pi\delta(E_1 + E_2 - E_f) \mathcal{N}_{d_1} \mathcal{N}_{d_2} \mathcal{N}_f \\ &\times c\epsilon^{ijk} 2(E_2 p_1^i - E_1 p_2^i) \chi_{d_1}^j \chi_{d_2}^k \\ &\times \int d\mathbf{R} d\mathbf{r} e^{i(\mathbf{p}_1 + \mathbf{p}_2) \cdot \mathbf{R}} e^{i\left(\frac{M_\alpha}{m_\eta + M_\alpha} \mathbf{p}_1 - \frac{m_\eta}{m_\eta + M_\alpha} \mathbf{p}_2\right) \cdot \mathbf{r}} \\ &\times \int \frac{d\mathbf{q}}{(2\pi)^3} F(\mathbf{q}) e^{-i\mathbf{q} \cdot \mathbf{r}} \phi_f^*(\mathbf{r}) e^{-i\mathbf{p}_f \cdot \mathbf{R}}. \end{aligned}$$

The integral in terms of \mathbf{R} provides momentum conservation

$$\int d\mathbf{R} e^{i(\mathbf{p}_1 + \mathbf{p}_2 - \mathbf{p}_f) \cdot \mathbf{R}} = (2\pi)^3 \delta(\mathbf{p}_1 + \mathbf{p}_2 - \mathbf{p}_f). \quad (9)$$

Introducing the Fourier transform

$$\phi_f(\mathbf{r}) = \int \frac{d\mathbf{p}}{(2\pi)^3} \tilde{\phi}_f(\mathbf{p}) e^{-i\mathbf{p} \cdot \mathbf{r}}, \quad (10)$$

we perform the spacial integrals and obtain

$$\begin{aligned} S &= -i(2\pi)^4 \delta^{(4)}(p_1 + p_2 - p_f) \mathcal{N}_{d_1} \mathcal{N}_{d_2} \mathcal{N}_f \\ &\times c\epsilon^{ijk} 2(E_2 p_1^i - E_1 p_2^i) \chi_{d_1}^j \chi_{d_2}^k \\ &\times \int \frac{d\mathbf{q}}{(2\pi)^3} F(\mathbf{q}) \tilde{\phi}_f^*(\mathbf{P}), \end{aligned} \quad (11)$$

where \mathbf{P} is defined as $\mathbf{P} = \frac{M_\alpha}{m_\eta + M_\alpha} \mathbf{p}_1 - \frac{m_\eta}{m_\eta + M_\alpha} \mathbf{p}_2 - \mathbf{q}$.

In the center of mass frame, $E_1 = E_2 \equiv E_d$ and $\mathbf{p}_1 = -\mathbf{p}_2 \equiv \mathbf{p}$. Since the T matrix is given by $S = 1 - iT(2\pi)^4 \delta^{(4)}(p_1 + p_2 - p_f) \mathcal{N}_{d_1} \mathcal{N}_{d_2} \mathcal{N}_f$, we obtain the T -matrix in the center of mass frame as

$$T = 4cE_d \mathbf{p} \cdot (\chi_{d_1} \times \chi_{d_2}) \tilde{F}(\mathbf{p}), \quad (12)$$

where we have defined $\tilde{F}(\mathbf{p})$ as

$$\tilde{F}(\mathbf{p}) \equiv \int \frac{d\mathbf{q}}{(2\pi)^3} F(\mathbf{q}) \tilde{\phi}_f^*(\mathbf{p} - \mathbf{q}). \quad (13)$$

With this T -matrix the cross section of the fusion with η production can be obtained as

$$d\sigma = \frac{1}{9} \sum_{\chi_{d_1}, \chi_{d_2}, f} \frac{|T|^2}{8p_{c.m.} E_d} (2\pi)^4 \delta^{(4)}(p_i - p_f) \frac{d\mathbf{p}_f}{(2\pi)^3 2E_f}, \quad (14)$$

where $p_{c.m.} = |\mathbf{p}|$ and we take average for the initial spin and sum up all the possible final states. Performing the integral in terms of \mathbf{p}_f and taking spin sum, we obtain

$$\sigma = \frac{2\pi}{9} c^2 p_{c.m.} \sum_f |\tilde{F}(\mathbf{p})|^2 \delta(E_i - E_f), \quad (15)$$

where we have used $E_i = 2E_d = E_f$.

The total cross section can be written with the Green's function of the η meson. Using Eq.(13), we have

$$\begin{aligned} &\sum_f |\tilde{F}(\mathbf{p})|^2 \delta(E_f - E_i) \\ &= \frac{1}{(2\pi)^6} \sum_f \delta(E_f - E_i) \int d\mathbf{q}_1 d\mathbf{r}_1 F(\mathbf{q}_1) e^{-i(\mathbf{q}_1 - \mathbf{p}) \cdot \mathbf{r}_1} \phi_f^*(\mathbf{r}_1) \\ &\quad \times \int d\mathbf{q}_2 d\mathbf{r}_2 F^*(\mathbf{q}_2) e^{i(\mathbf{q}_2 - \mathbf{p}) \cdot \mathbf{r}_2} \phi_f(\mathbf{r}_2). \end{aligned} \quad (16)$$

The sum over the final states provides the inclusive spectrum and can be evaluated by using Green's function method as follows: Using the formula $\delta(x) = -\frac{1}{\pi} \text{Im} \frac{1}{x + i\epsilon}$ for an infinitesimal quantity ϵ , we obtain

$$\begin{aligned} &\sum_f \delta(E_f - E_i) \phi_f^*(\mathbf{r}_1) \phi_f(\mathbf{r}_2) \\ &= -\frac{1}{\pi} \text{Im} \sum_f \phi_f^*(\mathbf{r}_1) \frac{1}{E_f - E_i + i\epsilon} \phi_f(\mathbf{r}_2) \end{aligned} \quad (17)$$

$$= -\frac{1}{\pi} \text{Im} \sum_f \phi_f^*(\mathbf{r}_1) \frac{1}{\hat{H} - E_i + i\epsilon} \phi_f(\mathbf{r}_2), \quad (18)$$

where we have used the fact that the wave function $\phi_f(\mathbf{r})$ is an eigenfunction of the Hamiltonian \hat{H} for the η - α system. Equation (18) is an representation of Green's operator $(\hat{H} - E_i + i\epsilon)^{-1}$ in terms of the eigenfunction of the Hamiltonian. Thus, we write the Green's function in the coordinate space as $G(E_i; \mathbf{r}_1, \mathbf{r}_2)$, and we have

$$\begin{aligned} \sigma &= \frac{2}{9} c^2 p_{c.m.} \\ &\times (-) \text{Im} \int d\mathbf{r}_1 d\mathbf{r}_2 f(\mathbf{r}_1) e^{i\mathbf{p} \cdot \mathbf{r}_1} G(E_i; \mathbf{r}_1, \mathbf{r}_2) f^*(\mathbf{r}_2) e^{-i\mathbf{p} \cdot \mathbf{r}_2}, \end{aligned} \quad (19)$$

where we have introduced the coordinate space expression of $F(\mathbf{q})$ as

$$f(\mathbf{r}) \equiv \int \frac{d\mathbf{q}}{(2\pi)^3} F(\mathbf{q}) e^{-i\mathbf{q} \cdot \mathbf{r}}. \quad (20)$$

Further by assuming the spherically symmetric form of f for simplicity, we replace $f(\mathbf{r})$ as,

$$f(\mathbf{r}) \rightarrow f(r). \quad (21)$$

And by making use of the multipole expansion of G ,

$$G(E_i; \mathbf{r}_1, \mathbf{r}_2) = \sum_{\ell m} Y_{\ell m}(\hat{r}_1) Y_{\ell m}^*(\hat{r}_2) G^\ell(E_i; r_1, r_2), \quad (22)$$

we obtain the final form of σ as,

$$\sigma = -\frac{8\pi}{9}c^2 p_{c.m.} \operatorname{Im} \int r_1^2 dr_1 r_2^2 dr_2 f(r_1) f^*(r_2) \times \sum_{\ell} (2\ell + 1) j_{\ell}(pr_1) G^{\ell}(E_i; r_1, r_2) j_{\ell}(pr_2), \quad (23)$$

where j_{ℓ} is the spherical Bessel function. This expression is used for the numerical evaluation of the fusion cross section of Eq. (15).

We can divide the total cross section σ into two parts, the conversion part σ_{conv} and the escape part σ_{esc} as,

$$\sigma = \sigma_{\text{conv}} + \sigma_{\text{esc}}, \quad (24)$$

based on the identity

$$\operatorname{Im}G = \{G^{\dagger} \operatorname{Im}UG\} + \{(1 + G^{\dagger}U^{\dagger}) \operatorname{Im}G_0(1 + UG)\}, \quad (25)$$

where G_0 is the free Green's function of η and U the η -nucleus potential [40]. The first term of the R.H.S of Eq. (25) represents the contribution of the η meson absorption by the imaginary part of the η -nucleus potential U and is called as the conversion part. The second term is the contribution from the η meson escape from the nucleus and is called as the escape part.

The conversion part of the cross section σ_{conv} is evaluated by the practical form written as,

$$\sigma_{\text{conv}} = -\frac{8\pi}{9}c^2 p_{c.m.} \int r_1^2 dr_1 r_2^2 dr_2 r_3^2 dr_3 f(r_1) f^*(r_3) \times \operatorname{Im}U_{\text{opt}}(r_2) \sum_{\ell} (2\ell + 1) j_{\ell}(pr_1) \times G^{\ell*}(E_i; r_1, r_2) G^{\ell}(E_i; r_2, r_3) j_{\ell}(pr_3), \quad (26)$$

for the spherical η - α optical potential $U_{\text{opt}}(r)$. We calculate the escape part as $\sigma_{\text{esc}} = \sigma - \sigma_{\text{conv}}$.

The conversion and escape parts have the different energy dependence. In the subthreshold energy region of the η meson production, the total cross section σ is equal to the conversion part σ_{conv} since the energy of the η meson is insufficient to escape from the nucleus and all η mesons must be absorbed to the nucleus finally. Thus, the signal of the formation of the η bound state is expected to be observed in σ_{conv} . As shown in Eq. (26), the expression of the conversion cross section σ_{conv} includes the Green's function G^{ℓ} which is responsible for the peak and cusp structures in the spectrum as the consequences of the η -nucleus interaction such as the bound state formation with angular momentum ℓ . For higher partial waves ℓ without any bound states, the energy dependence of G^{ℓ} is tend to be rather mild and almost flat in the energy region of the η production threshold. In addition, σ_{conv} also includes $\operatorname{Im}U_{\text{opt}}$ and, thus, the size of σ_{conv} will be larger for stronger absorptive potential. Consequently, as shown later, the flat contribution to the conversion spectrum gets larger in proportional to the strength of the absorptive potential. Above the threshold of η production, we have also the contribution from the escape processes. This escape

part σ_{esc} can be compared to the observed η production cross section in the $d + d \rightarrow \eta + \alpha$ reaction.

We should mention here to the effects of the distortion of the initial deuterons to the calculated results. In Eq. (3), the deuteron waves are introduced to the formula as plane waves. The distortion effects will modify the deuteron-deuteron relative wave function and could change the results. In the present cases, however, we can expect the effects will be minor in the final spectra shown in next section by the following reasons. The energy range of the final spectra considered in this article is very narrow and restricted to only around the η production threshold. Thus, the distortion effects between two deuterons are almost constant in this narrow energy range and are expected to change only absolute value of the spectra by an almost constant factor. On the other hand, in the present analyses, we normalize the calculated results using the experimental data of $d + d \rightarrow \eta + \alpha$ reaction observed above the threshold as we will see later. Thus, the final results are expected to be insensitive to the deuteron distortion. We have checked qualitatively this statement by introducing the spherical distortion factor to suppress the contributions from the small relative coordinate region in Eqs. (23) and (26), and we have confirmed that the distortion effects to the spectra is almost constant within the accuracy of around 15 % in the energy region considered here. Hence, we can neglect the deuteron distortion effects in this article.

As for the numerical evaluation, we assume the η - α optical potential has the following form,

$$U_{\text{opt}}(r) = (V_0 + iW_0) \frac{\rho_{\alpha}(r)}{\rho_{\alpha}(0)}, \quad (27)$$

where V_0 and W_0 are the parameters to determine the potential strength at center of the α particle. The density of the α particle $\rho_{\alpha}(r)$ is assumed to have Gaussian form,

$$\rho_{\alpha}(r) = \rho_{\alpha}(0) \exp\left[-\frac{r^2}{a^2}\right], \quad (28)$$

with the range parameter $a = 1.373$ fm which reproduces the R.M.S radius of α to be 1.681 fm. The central density of this distribution is $\rho_{\alpha}(0) = 0.28 \text{ fm}^{-3} \simeq 1.6\rho_0$ with the normal nuclear density $\rho_0 = 0.17 \text{ fm}^{-3}$. As the practical form of F , we assume the Gaussian as,

$$F(\mathbf{p}) = (2\pi)^{3/2} \left(\frac{2}{p_0^2\pi}\right)^{3/4} \exp\left[-\frac{p^2}{p_0^2}\right], \quad (29)$$

in this article and we treat p_0 as a phenomenological parameter. We also show the numerical results obtained by choosing other functional forms for the transition form factor $F(\mathbf{p})$ ($f(\mathbf{r})$) in Appendix to estimate the functional form dependence of our results.

We make a few comments on the difficulties for developing more microscopic model to evaluate the reaction rate. The first difficulty is the large momentum transfer. We need around 1 GeV/c momentum transfer at the η production threshold in the center of mass frame. The

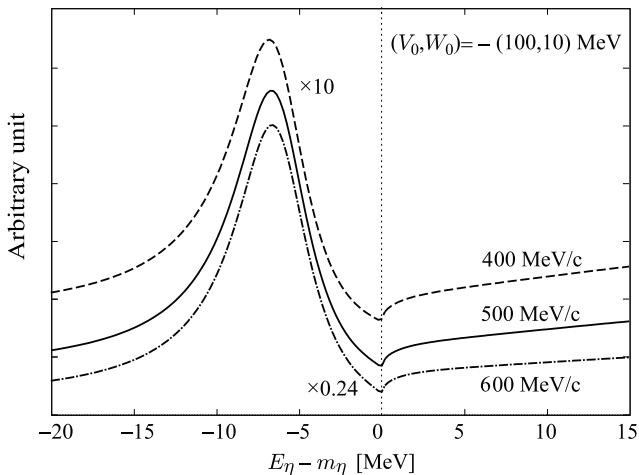


Fig. 2. Calculated total cross sections of the $d + d \rightarrow (\eta + \alpha) \rightarrow X$ reaction for the formation of the η - α bound system with $p_0 = 400, 500, 600$ MeV/ c cases plotted as functions of the η excited energy $E_\eta - m_\eta$. The parameters of the η - α optical potential are fixed to be $(V_0, W_0) = -(100, 10)$ MeV. It is noted that the result with $p_0 = 600$ MeV/ c is scaled by factor 0.24 and that with $p_0 = 400$ MeV/ c scaled by factor 10.

accuracy of the microscopic wave function in such high momentum transfer region is not well investigated. Another difficulty arises from the fact that the reaction is a fusion reaction. In the fusion reaction, all particles in the system participate the reaction equally and receive large momentum transfer. Because of these features of this reaction, we need the sufficiently accurate wave function of the five-body system (four nucleons and one η meson) and the reliable description of the fusion and η production processes to perform the fully microscopic calculation.

On the other hand, at the same time, we can also find an advantage for the studies of this reaction. We can make use of the experimental data of the $d + d \rightarrow \eta + \alpha$ reaction just above the η production threshold [37,38,39]. These data must provide us important information on the reaction and can be used to fix the parameters included in the present model. It should be also mentioned that the energy spectrum of the η - α system is expected to be simple since the system is small and may have only a few bound levels of η even if they exist. The simple spectrum could be helpful to identify the bound levels from the data.

3 Numerical Results and Discussions

The theoretical model described in section 2 includes three parameters, which are the strength of the real and imaginary parts of the η - α potential (V_0, W_0) defined in Eq. (27), and the parameter p_0 appeared in Eq.(29) to determine the property of the function F which physical meanings are explained in Eqs. (1) and (2).

We study first the sensitivity of the shape of the cross section to the parameter p_0 . We show the calculated total cross section σ in Eq. (23) for $p_0 = 400, 500, 600$ MeV/ c

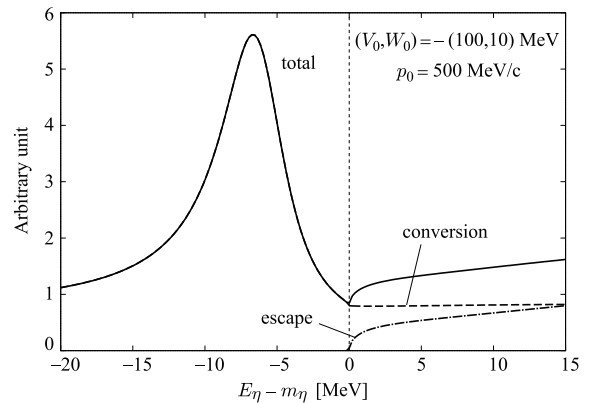


Fig. 3. Calculated cross section of the $d + d \rightarrow (\eta + \alpha) \rightarrow X$ reaction for the formation of the η - α bound system plotted as functions of the η excited energy $E_\eta - m_\eta$. The parameters of the η - α optical potential are $(V_0, W_0) = -(100, 10)$ MeV, and the parameter p_0 is fixed to be $p_0 = 500$ MeV/ c . The thick solid line indicates the total cross section σ . The dashed line and the dot-dashed line indicate the conversion part σ_{conv} and the escape part σ_{esc} , respectively.

cases with $(V_0, W_0) = -(100, 10)$ MeV as functions of the η excited energy $E_\eta - m_\eta$ in Fig. 2. The peak structure of the results with $p_0 = 400$ MeV/ c is small and is located on the top of almost flat spectrum. We find that the structures appearing in the cross section is insensitive to p_0 and almost same for three p_0 values. Thus, we fix the value of this parameter to be $p_0 = 500$ MeV/ c in the following numerical results and focus on the sensitivity of the structure of the spectrum to the η - α potential strength.

The parameter p_0 dependence of the total cross section can be understood by considering the change of spatial dimension of the $f(\mathbf{r})$ defined in Eq. (20). For smaller p_0 value, the distribution of F in the momentum space is more compact and that of f in coordinate space is wider. Thus, for smaller p_0 values, we have relatively larger contributions of higher partial wave ℓ of the η meson in the calculation of the cross section in Eq. (23), which are expected not to have any structures as function of energy around the threshold as mentioned before. Hence, for smaller p_0 values, the small peak structure appears on the top of the almost flat contribution in the spectrum.

In Fig. 3, we show again the calculated σ for the case with parameters $(V_0, W_0) = -(100, 10)$ MeV for $p_0 = 500$ MeV/ c to study the detail structure of the spectrum. Three lines correspond to the total cross section σ , the conversion part σ_{conv} , and the escape part σ_{esc} . The η production threshold corresponds to $E_\eta - m_\eta = 0$ and the η - α bound states are expected to be produced in the sub-threshold region $E_\eta - m_\eta < 0$. We can see in Fig. 3 that the spectrum has non-trivial structures above the flat contribution whose height seems to be about 1 in the scale of the vertical axis. There is a clear peak at $E_\eta - m_\eta \simeq -7$ MeV which corresponds to the formation of the η - α bound state. The calculated escape part is plotted with data in Fig. 4. We have adjusted the height of the spectrum by the interaction strength c in Eq. (1). The agreement of

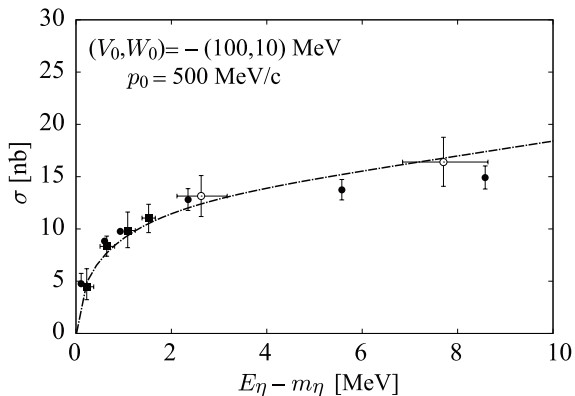


Fig. 4. Calculated escape part σ_{esc} in Fig. 3 plotted with the experimental data of $d + d \rightarrow \eta + \alpha$ reaction indicated by black squares [37], black circles [38], and open circles [39]. The parameters of the η - α optical potential are $(V_0, W_0) = -(100, 10)$ MeV and the parameter p_0 is fixed to be $p_0 = 500$ MeV/c. The height of the calculated spectrum is adjusted so as to reproduce the data by changing the interaction strength c given in Eq. (1).

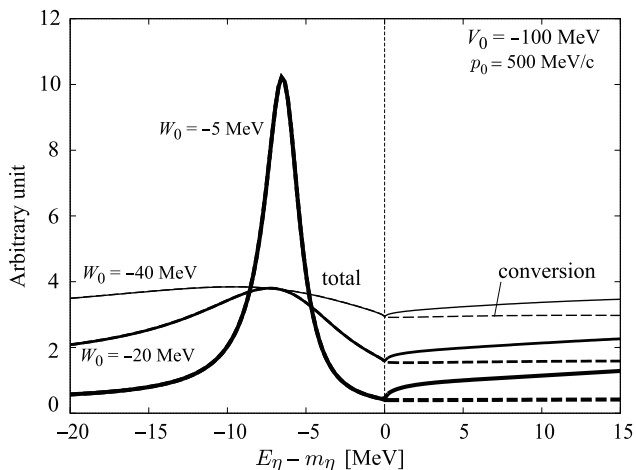


Fig. 5. Calculated cross sections of the $d + d \rightarrow (\eta + \alpha) \rightarrow X$ reaction for the formation of the η - α bound system plotted as functions of the η excited energy $E_\eta - m_\eta$. The parameters of the η - α optical potential are $(V_0, W_0) = -(100, 5)$, $-(100, 20)$, and $-(100, 40)$ MeV, and the parameter p_0 is fixed to be $p_0 = 500$ MeV/c. The solid lines indicate the total cross sections σ and the dashed lines the conversion parts σ_{conv} .

the spectrum shapes of the calculated results and the data above the threshold seems reasonably good in this potential parameter. Hence, this observation implies that this parameter set, which predicts the formation of η - α bound state, does not contradict to the $d + d \rightarrow \eta + \alpha$ data above threshold. We will make further comments for the comparison with the subthreshold data later in this section.

In Fig. 5, we show the results for $(V_0, W_0) = -(100, 5)$, $-(100, 20)$ and $-(100, 40)$ MeV cases with $p_0 = 500$ MeV/c to see the effects of the strength of the imaginary poten-

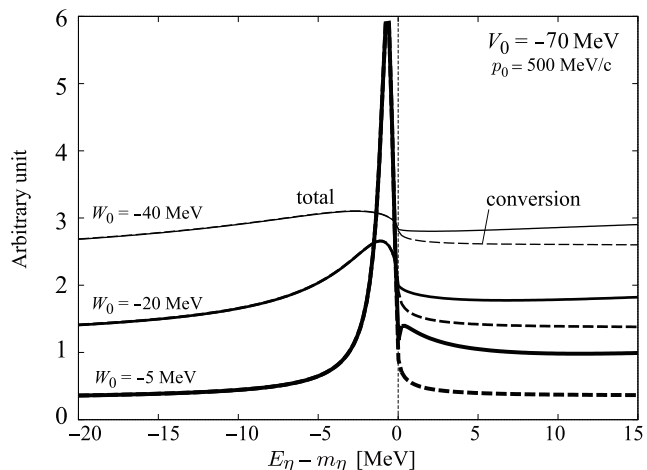


Fig. 6. Same as Fig. 5 except for $(V_0, W_0) = -(70, 5)$, $-(70, 20)$, and $-(70, 40)$ MeV.

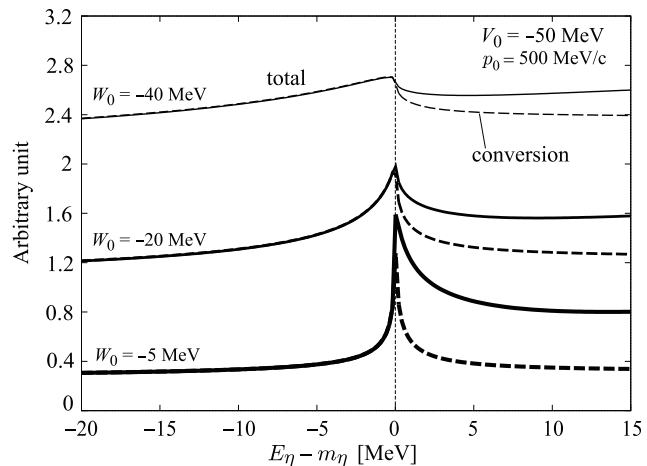


Fig. 7. Same as Fig. 5 except for $(V_0, W_0) = -(50, 5)$, $-(50, 20)$, and $-(50, 40)$ MeV.

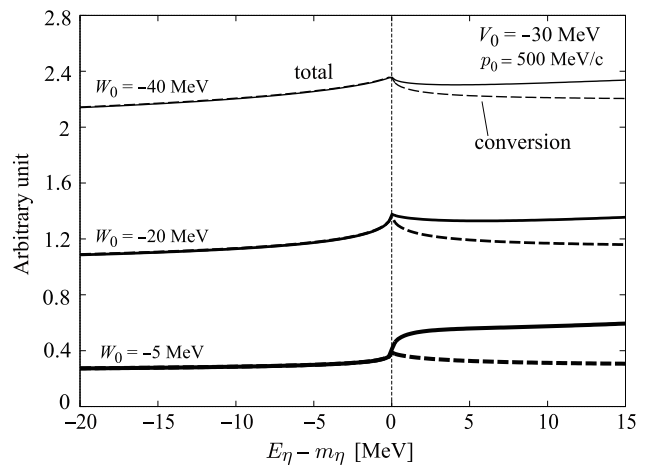


Fig. 8. Same as Fig. 5 except for $(V_0, W_0) = -(30, 5)$, $-(30, 20)$, and $-(30, 40)$ MeV.

tial W_0 to the spectra. We can see from the figures the structure of the spectra below threshold $E_\eta - m_\eta < 0$ is sensitive to the value of the potential parameters W_0 and is expected to be the good observables to investigate the η -nucleus interaction. Actually, the subthreshold spectrum with small imaginary potential $W_0 = -5$ MeV clearly shows the existence of the bound state around $E_\eta - m_\eta = -7$ MeV as a peak structure. The width of the peak becomes wider and the peak height lower for larger $|W_0|$ value. At the same time we can see that the structure of the spectra above the threshold $E_\eta - m_\eta > 0$ are relatively insensitive to the imaginary part of the η -nucleus interaction and the value of W_0 .

We also show the calculated results for different V_0 and W_0 values in Figs. 6, 7 and 8. It could be interesting to note that the depth of the η -nucleus potential by the chiral unitary model in Refs. [12,13] is roughly close to $-(50, 40)$ MeV at normal nuclear density for real and imaginary parts, respectively. The depth of the so-called $t\rho$ potential evaluated by using the η - N scattering length $a_{\eta N} = (0.28 + 0.19i)$ fm in Ref. [41] is around $-(30, 20)$ MeV at normal nuclear density. It should be noted that the parameters V_0 and W_0 adopted here in Eq. (27) indicate the potential strength at the center of the α -particle where $\rho_\alpha(0) \simeq 0.28 \text{ fm}^{-3}$ as defined in Eq. (28). The η - α potential also has been studied microscopically in Refs. [42,43,44], where the various values of the η - α scattering length $a_{\eta\alpha}$ were reported. We could compare our potential strength (V_0, W_0) with the scattering length simply by the Born approximation as $a_{\eta\alpha} = -2\mu \int dr r^2 U_{\text{opt}}(r)$ with the η - α reduced mass μ . For example, based on this relation, some of the potential parameters used in this article correspond to the scattering length as,

$$\begin{aligned} (V_0, W_0) = -(100, 5) \text{ MeV} &\leftrightarrow a_{\eta\alpha} = 2.81 + 0.14i \text{ fm} \\ (V_0, W_0) = -(70, 20) \text{ MeV} &\leftrightarrow a_{\eta\alpha} = 1.97 + 0.56i \text{ fm} \\ (V_0, W_0) = -(50, 40) \text{ MeV} &\leftrightarrow a_{\eta\alpha} = 1.40 + 1.12i \text{ fm}. \end{aligned}$$

It will be interesting to compare these numbers with the microscopic scattering lengths, for example, results of the microscopic calculation listed in Table IV in Ref. [44]. We can see that the potential strengths adopted in this article are within the range of uncertainties of microscopic calculation.

We find again the same tendencies in these results as in Fig. 5. In Fig. 6 for $V_0 = -70$ MeV case, we also find the bound state peak at $E_\eta - m_\eta \simeq -1$ MeV which is very clear for small $|W_0|$ case. In the result shown in Fig. 7 for $V_0 = -50$ MeV case, we find the cusp structure at the threshold energy, which becomes less prominent for larger absorption potential. In Fig. 8, for weaker attractive cases with $V_0 = -30$ MeV, we find the step like structure at the threshold for weak absorptive case with $W_0 = -5$ MeV, which becomes less prominent again for stronger absorptive potential with larger $|W_0|$ value. From these figures, we find that the total spectra around and below threshold $E_\eta - m_\eta \leq 0$ are sensitive to both the real and imaginary parts of the η -nucleus interaction described by the

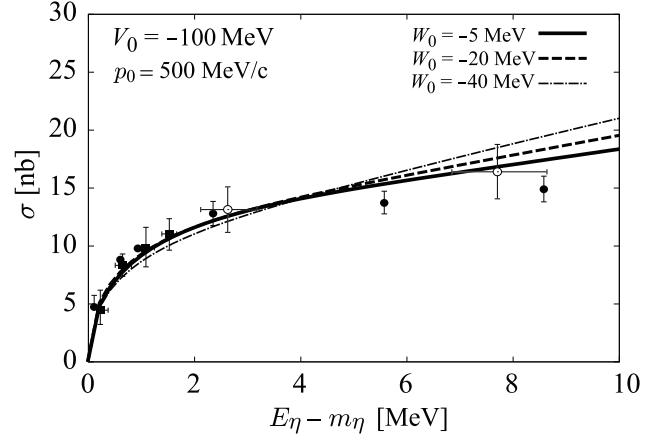


Fig. 9. Calculated escape part σ_{esc} plotted with the experimental data of $d + d \rightarrow \eta + \alpha$ reaction indicated by black squares [37], black circles [38], and open circles [39]. The parameters of the η - α optical potential are $(V_0, W_0) = -(100, 5)$, $-(100, 20)$, and $-(100, 40)$ MeV as shown in the figure. The parameter p_0 is fixed to be $p_0 = 500 \text{ MeV}/c$.

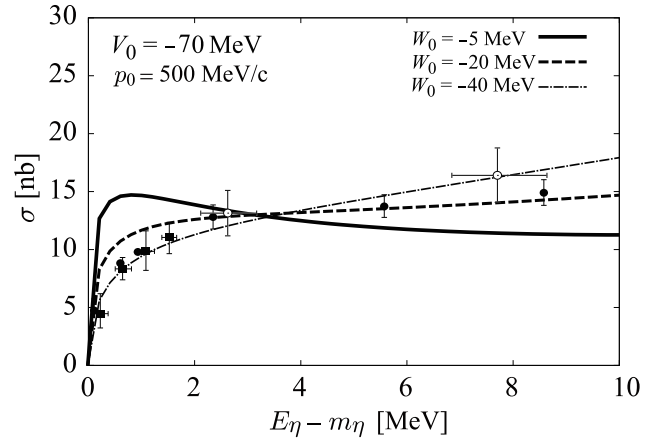


Fig. 10. Same as Fig. 9 except for the η - α optical potential parameters are $(V_0, W_0) = -(70, 5)$, $-(70, 20)$, and $-(70, 40)$ MeV as shown in the figure.

parameters (V_0, W_0) and are good observables to obtain information on the η -nucleus interaction.

As shown in the conversion spectra in Figs. 5–8, we have the almost flat contributions in whole energy region as mentioned in Sect. 2. This flat contribution is considered to be a part of the background cross sections of the experimental data. Thus, we subtract the flat contribution in the conversion part in the following numerical results to investigate the structure appearing in the spectrum. For this purpose, we subtract the minimum value of the conversion cross section in the energy range shown in the following figures.

It will be extremely interesting to show the binding energies and widths of the η - α bound states obtained by solving the Klein-Gordon equation using the same η - α potential used to calculate the spectra in Figs. 5–8. The results are compiled in Table 1. We find that only peak structures

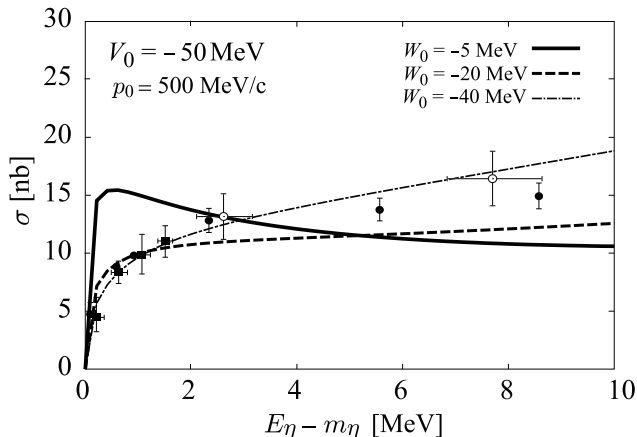


Fig. 11. Same as Fig. 9 except for the η - α optical potential parameters are $(V_0, W_0) = -(50, 5), -(50, 20),$ and $-(50, 40)$ MeV as shown in the figure.

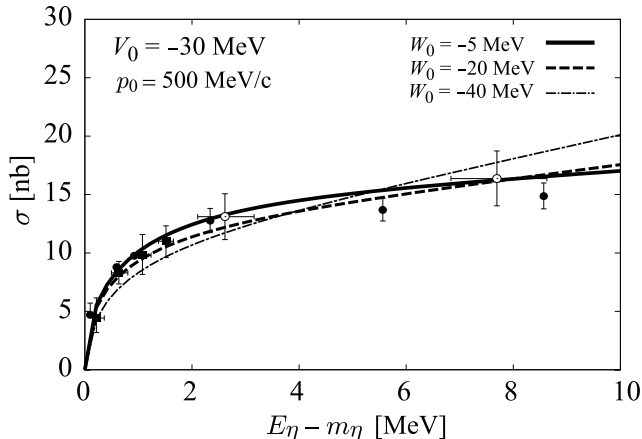


Fig. 12. Same as Fig. 9 except for the η - α optical potential parameters are $(V_0, W_0) = -(30, 5), -(30, 20),$ and $-(30, 40)$ MeV as shown in the figure.

appearing in the spectra for the strong attractive–weak absorptive potential cases correspond to the existence of the bound states. Other structures in the spectra may not indicate the existence of the bound state, though they provide important information on the η - α interaction definitely.

Now, we focus on the escape part of the spectrum which appears above the threshold, $E_\eta - m_\eta > 0$, and can be compared to the experimental data of the $d + d \rightarrow \eta + \alpha$ reaction as already shown in Fig. 4 for a certain parameter set. In Fig. 9, we show the calculated escape part of the spectra for $V_0 = -100$ MeV cases with different strengths of the absorptive potential together with the experimental data. The calculated results are scaled to fit the experimental data by changing the interaction strength c . As we can see from Figs. 4 and 9, the shape of the escape part is relatively insensitive to the value of the potential parameter W_0 in this case.

Table 1. Calculated binding energies (B.E.) and widths (Γ) of the η - α bound states by solving the Klein-Gordon equation with the optical potential defined in Eq. (27). All states shown here are ground states. We have not found any bound states for $V_0 = -50$ and -30 MeV with $W_0 = -5, -20, -40$ MeV cases.

W_0 [MeV]	$V_0 = -100$ MeV		$V_0 = -70$ MeV	
	B.E.	Γ	B.E.	Γ
-5	6.4	2.7	0.5	1.1
-20	5.7	11.0	-	-
-40	3.3	22.9	-	-

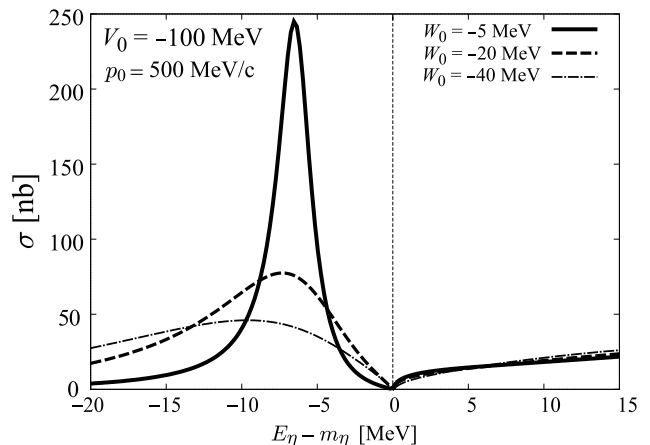


Fig. 13. Calculated total cross sections of $d + d \rightarrow (\eta + \alpha) \rightarrow X$ reaction scaled by the same factor used in Fig. 9 plotted as functions of the η excited energy $E_\eta - m_\eta$. The flat contributions are subtracted. The parameters of the η - α optical potential are $(V_0, W_0) = -(100, 5), -(100, 20),$ and $-(100, 40)$ MeV, and the parameter p_0 is fixed to be $p_0 = 500$ MeV/ c .

We also show the calculated results of the escape part with different potential parameters in Figs. 10, 11 and 12 for different strengths of the attractive potential. We find that the shape of the escape part is not very sensitive to the V_0 and W_0 parameters and that it could be uneasy to obtain the detail information on η -nucleus potential only from the escape parts. Although we have some cases which could be safely ruled out by these comparison, such as $(V_0, W_0) = -(70, 5)$ and $-(50, 5)$ MeV cases, in which we find a distinct threshold structure as shown in Figs. 10 and 11, the whole shape of the calculated results are not so much different from that of experimental data in many cases.

One of the best ways to obtain the decisive information on the η -nucleus interaction may be to have the direct experimental observation of the η -nucleus spectrum below the threshold, where the spectrum shape is more sensitive to the potential parameters as shown in Figs. 5–8, especially if a bound state exists. Nevertheless, it could happen that nature might not give us any bound states or our experimental techniques would not be sufficient to distinguish a less prominent peak due to a large width. In such cases, we could deduce the information on the

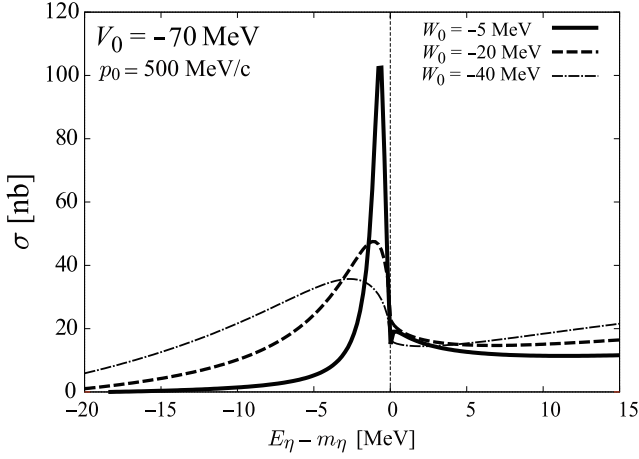


Fig. 14. Calculated total cross sections of $d+d \rightarrow (\eta+\alpha) \rightarrow X$ reaction scaled by the same factor used in Fig. 10 plotted as functions of the η excited energy $E_\eta - m_\eta$. The flat contributions are subtracted. The parameters of the η - α optical potential are $(V_0, W_0) = -(70, 5)$, $-(70, 20)$, and $-(70, 40)$ MeV, and the parameter p_0 is fixed to be $p_0 = 500$ MeV/ c .

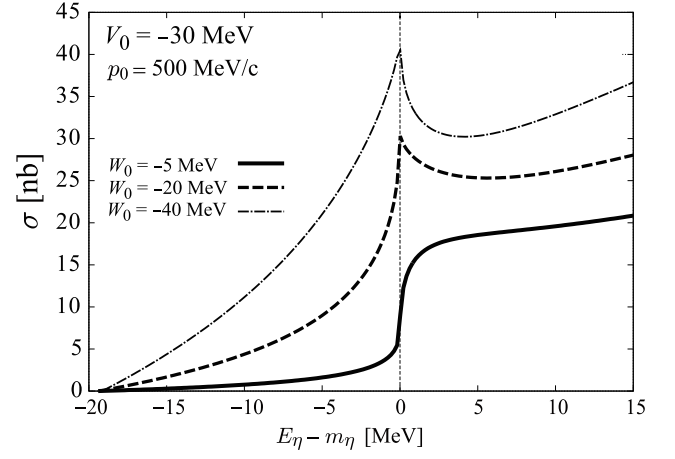


Fig. 16. Calculated total cross sections of $d+d \rightarrow (\eta+\alpha) \rightarrow X$ reaction scaled by the same factor used in Fig. 12 plotted as functions of the η excited energy $E_\eta - m_\eta$. The flat contributions are subtracted. The parameters of the η - α optical potential are $(V_0, W_0) = -(30, 5)$, $-(30, 20)$, and $-(30, 40)$ MeV, and the parameter p_0 is fixed to be $p_0 = 500$ MeV/ c .

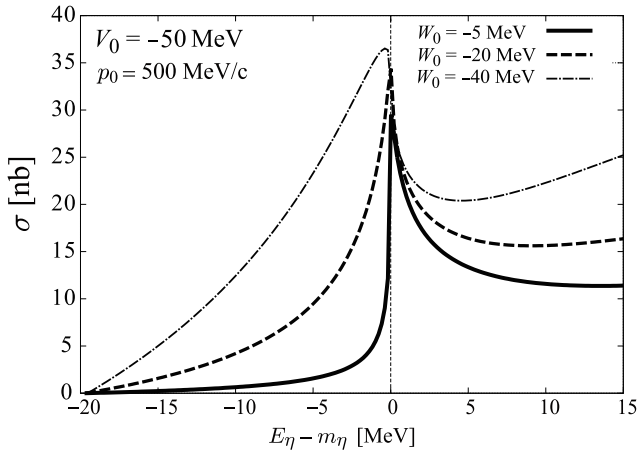


Fig. 15. Calculated total cross sections of $d+d \rightarrow (\eta+\alpha) \rightarrow X$ reaction scaled by the same factor used in Fig. 11 plotted as functions of the η excited energy $E_\eta - m_\eta$. The flat contributions are subtracted. The parameters of the η - α optical potential are $(V_0, W_0) = -(50, 5)$, $-(50, 20)$, and $-(50, 40)$ MeV, and the parameter p_0 is fixed to be $p_0 = 500$ MeV/ c .

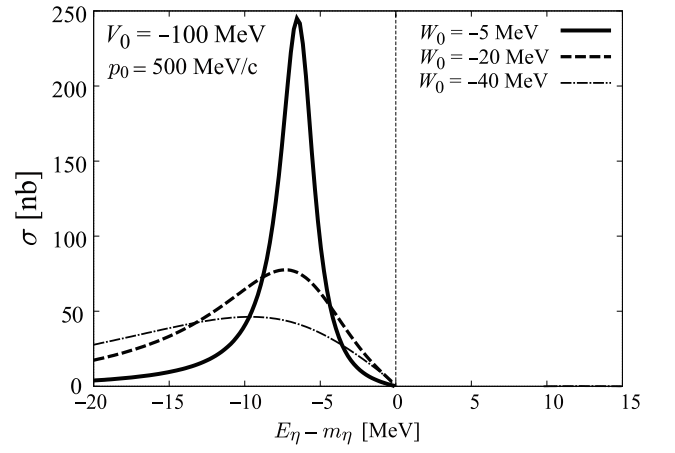


Fig. 17. Calculated conversion part of cross sections of $d+d \rightarrow (\eta+\alpha) \rightarrow X$ reaction scaled by the same factor used in Fig. 9 plotted as functions of the η excited energy $E_\eta - m_\eta$. The flat contributions are subtracted. The parameters of the η - α optical potential are $(V_0, W_0) = -(100, 5)$, $-(100, 20)$, and $-(100, 40)$ MeV, and the parameter p_0 is fixed to be $p_0 = 500$ MeV/ c .

η -nucleus interaction from the absolute value of the spectrum below the η -nucleus threshold in comparison with the η production cross section in the same reaction above the threshold.

Here we have a model which can be used to calculate both the conversion and escape parts in the same footing simultaneously. The conversion part describes the spectrum shape induced by the η absorption to the nucleus, while the escape part shows the η production cross section. In our model, we leave the interaction strength of the $d+d \rightarrow \eta+\alpha$ given in Eq. (1) as a free parameter. We can adjust this parameter so as to reproduce the η production data by the escape part of our spectrum,

and then the conversion part can be an outcome from the model. Since the conversion part of the spectrum below the threshold is more sensitive to the η -nucleus interaction parameters, comparing the theoretical prediction and experimental data of the $d+d$ reaction below the threshold, we can deduce the information on the interaction parameters.

For the purpose, we show the scaled theoretical total cross section of the $d+d \rightarrow (\eta+\alpha) \rightarrow X$ reaction in Figs. 13–16 for various values of the parameter (V_0, W_0) . The absolute value of the cross section in these figures are determined so that the escape part of the cross section reproduces the experimental data of $d+d \rightarrow \eta+\alpha$

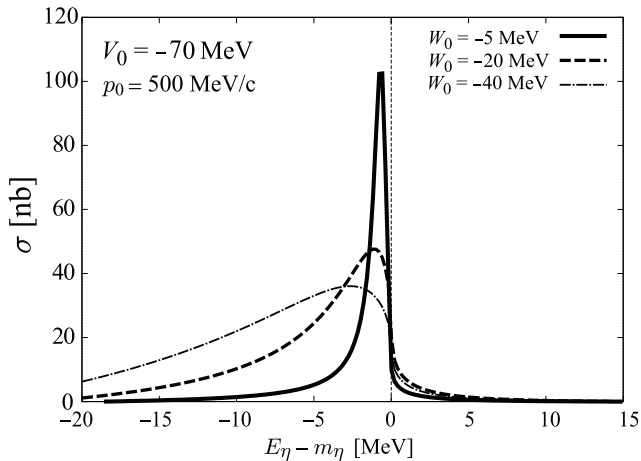


Fig. 18. Calculated conversion part of cross sections of $d + d \rightarrow (\eta + \alpha) \rightarrow X$ reaction scaled by the same factor used in Fig. 10 plotted as functions of the η excited energy $E_\eta - m_\eta$. The flat contributions are subtracted. The parameters of the η - α optical potential are $(V_0, W_0) = -(70, 5)$, $-(70, 20)$, and $-(70, 40)$ MeV, and the parameter p_0 is fixed to be $p_0 = 500$ MeV/ c .

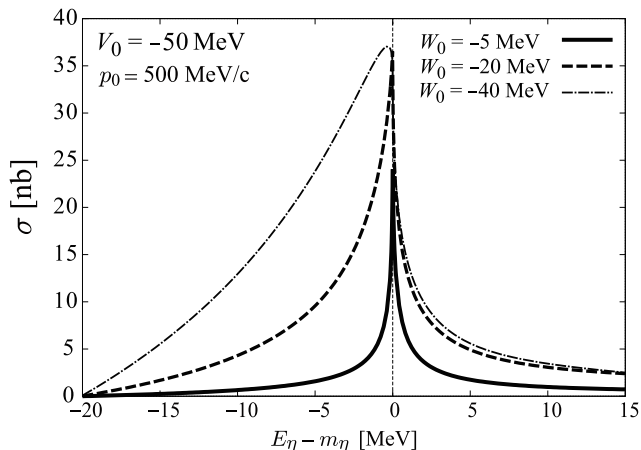


Fig. 19. Calculated conversion part of cross sections of $d + d \rightarrow (\eta + \alpha) \rightarrow X$ reaction scaled by the same factor used in Fig. 11 plotted as functions of the η excited energy $E_\eta - m_\eta$. The flat contributions are subtracted. The parameters of the η - α optical potential are $(V_0, W_0) = -(50, 5)$, $-(50, 20)$, and $-(50, 40)$ MeV, and the parameter p_0 is fixed to be $p_0 = 500$ MeV/ c .

and the nonstructural flat contributions described above are subtracted in the conversion part. We should mention here that the structure of the spectra in these figures is enhanced for smaller $|W_0|$ values in Figs. 13 and 14, while it is suppressed for smaller $|W_0|$ values in Figs. 15 and 16. This behavior can be understood by considering the origin of the structure of the spectrum. For the strong attractive potential cases, since the structure is dominated by the peak due to the existence of the bound state, the peak structure becomes more prominent for the weaker imaginary because of the smaller width of the bound state. On

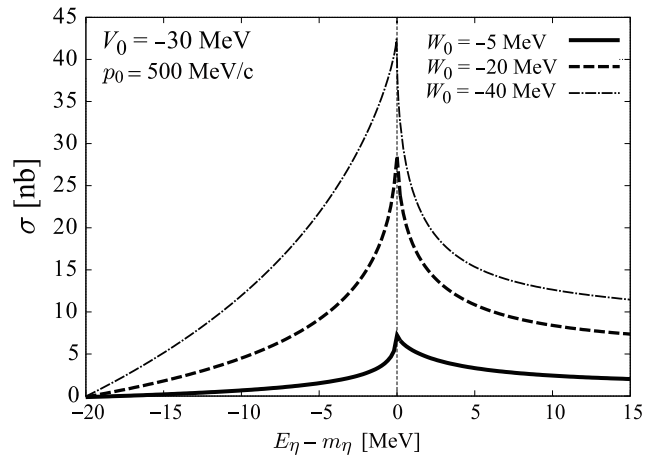


Fig. 20. Calculated conversion part of cross sections of $d + d \rightarrow (\eta + \alpha) \rightarrow X$ reaction scaled by the same factor used in Fig. 12 plotted as functions of the η excited energy $E_\eta - m_\eta$. The flat contributions are subtracted. The parameters of the η - α optical potential are $(V_0, W_0) = -(30, 5)$, $-(30, 20)$, and $-(30, 40)$ MeV, and the parameter p_0 is fixed to be $p_0 = 500$ MeV/ c .

the other hand, for the weak real potential cases, since the structure is dominated by the absorptive processes, the structure can be suppressed for the weaker absorptive potentials.

For comparison of our calculated results with experimental data for the subthreshold energies, we show only the conversion part, since in experiment the system energy is measured by observing a pion, nucleon and a residual nucleus emitted due to η absorption and this process is counted in the conversion part in the calculation. In Figs. 17–20, we show the calculated conversion parts of the spectra which correspond to the η absorption processes. The obtained spectra shown in Figs. 17–20 can be compared to the shape of the experimental spectra on the background reported in Ref. [35], where the upper limit of the peak structure of the $d + d \rightarrow {}^3\text{He} + n + \pi^0$ is 3–6 nb. This implies that the experimental upper limit for the semi-inclusive conversion spectrum of $d + d \rightarrow (\eta + \alpha) \rightarrow {}^3\text{He} + N + \pi$ including both $n + \pi^0$ and $p + \pi^-$ channel could be estimated to be 3–6 nb \times 3 = 9–18 nb because of the isospin symmetry of the decay channel of the η - α system. In this case, the peak structures of the bound states in Figs. 17 and 18 are fully rejected and strong attractive with less absorptive potentials are not allowed. In addition, the upper limit provides the strong restriction to the η - α potential and only weak potential cases with small $|V_0|$ and $|W_0|$ values such as $(V_0, W_0) = -(50, 5)$ and $-(30, 5)$ cases could be allowed by the limit.

In order to understand the meaning of the experimental upper limit and the results of our analyses more clearly, we plot a contour plot of the height of the structure appeared in the conversion spectra on the flat contribution in the $V_0 - W_0$ plane in Fig. 21, where the acceptable region of V_0, W_0 values can be easily understood for each value of the upper limit of the height of the structure in

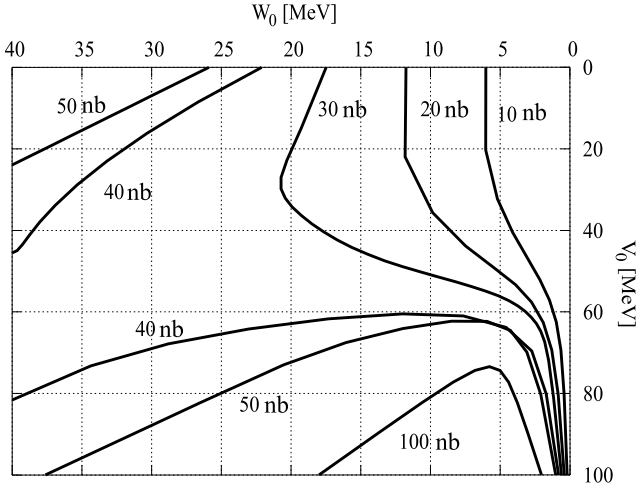


Fig. 21. Contour plot of the height of the structure appearing in the conversion spectra such as shown in Figs. 17–20 in the $V_0 - W_0$ plane. This plot shows clearly the acceptable region of the potential strength for various values of the upper limit of the height of the structure in the $d + d \rightarrow {}^3\text{He} + N + \pi$ reaction.

the conversion spectra such as shown in Figs. 17–20. From this figure, the upper limit reported in Ref. [35] is found to provide very valuable information on η -nucleus interaction and strongly suggests the small $|V_0|$ and $|W_0|$ values. However, it should be noted that the results in Fig. 21 are considered to be qualitative since we have not considered the experimental energy resolution here. In addition, the shapes of the structure appearing in Figs. 17–20 are not simply the symmetric peak. We also need to understand the origin of the absorptive potential and branching ratio of various decay processes to compare our results to the data for the specific decay mode. Actually, we have only considered one-nucleon absorption process for η meson here. Multi-nucleon processes are also possible in reality [45]. Thus, for deducing the quantitative information on η -nucleus interaction, it is mandatory to make the detail comparison between the calculated results and data by taking account of the realistic experimental energy resolution, asymmetric shape of the structure appeared in the conversion spectra, the branching ratio of the decay process of η bound states and so on, especially for sub-threshold energy region, where the spectra may have variety of structures depending on the η -nucleus interaction strength.

Finally, we mention the effects of the possible energy dependence of the optical potential. The optical potential has the energy dependence in general and the dependence could change the calculated spectra. To simulate the energy dependence of η - α optical potential, we adopted the energy dependence of the η -nucleon scattering length in Ref. [46] and we assumed the η -nucleon relative energy to be the quarter of that of the η - α . The potential strength are normalized at the threshold energy. The calculated results are shown in Figs. 22 and 23. We have found that the energy dependence of the imaginary part of the optical potential mainly affects the strength of the conversion part

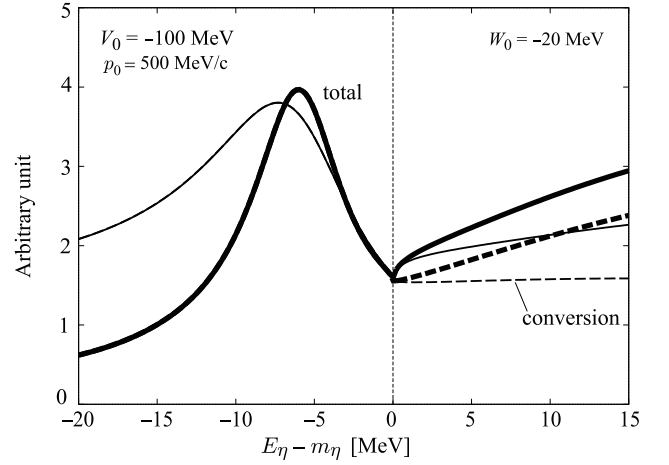


Fig. 22. Calculated cross sections of the $d + d \rightarrow (\eta + \alpha) \rightarrow X$ reaction for the formation of the $\eta - \alpha$ bound system plotted as functions of the η excited energy $E_\eta - m_\eta$. The parameters of the η - α optical potential is $(V_0, W_0) = -(100, 20)$ MeV, and the parameter p_0 is fixed to be $p_0 = 500$ MeV/ c . The solid lines indicate the total cross sections σ and the dashed lines the conversion parts σ_{conv} . The thin lines are the results with the energy independent optical potential and the thick lines are those with the energy dependent optical potential (see text).

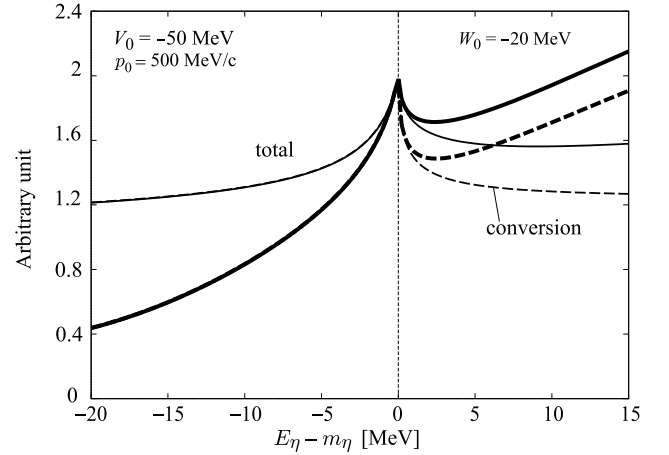


Fig. 23. Same as Fig. 22 except for $(V_0, W_0) = -(50, 20)$ MeV.

in the spectra and changes the flat contribution of conversion part to the slope with some gradient. Hence, this effect could be important for the more realistic analyses. Though, there are many theoretical models for η -nucleon scattering length as compiled in Ref. [47], the qualitative features seems common for all models.

4 Conclusion

We have developed a theoretical model to evaluate the formation rate of the η - α bound states in the $d + d$ fusion reaction. Because of the difficulties due to the large momentum transfer which is unavoidable to produce η meson

in the fusion reaction, we formulate the model in a phenomenological way. We have shown the numerical results for the cases with the various sets of the η -nucleus interaction parameters.

We have found that the data of η production above threshold provide important information on the absolute strength of the reaction by comparing them with the escape part of the calculated results. The upper limit of the formation cross section of the η mesic nucleus reported in Ref. [33] also provides the significant information on the strength of the η -nucleus interaction. We would like to stress here that simultaneous fit to both data of $d + d \rightarrow \eta + \alpha$ and $d + d \rightarrow (\eta + \alpha) \rightarrow X$ using our model make it possible to provide valuable information on η -nucleus interaction. The results of our analyses are compiled in Fig. 21 as a contour plot of the $V_0 - W_0$ plane.

The present discussion is simply based on the value of the upper limit of the peak structure in the fusion reaction spectrum below the threshold. As for the further works, to make the analyses performed in this article more quantitative and developed, direct comparison of the spectrum shapes between the calculated results and experiments should be necessary. For this purpose, we should take account of experimental energy resolution in the calculation and consider other possibilities of the shapes of the spectrum structure by improving the η -nucleus optical potential.

We acknowledge the fruitful discussion with P. Moskal, W. Krzemien, and M. Skurzok. S. H. thanks A. Gal, N. G. Kelkar, S. Wycech, E. Oset and V. Metag for fruitful comments and discussion in Krakow. We also thank K. Itahashi and H. Fujioka for many discussions and collaborations on meson-nucleus systems. This work was partly supported by JSPS KAKENHI Grant Numbers JP24540274 and JP16K05355 (S.H.), 17K05443 (H.N.), JP15H06413 (N.I.), and JP17K05449 (D.J.) in Japan.

A Appendix

In this appendix, we show the numerical results for the different functional form of the transition form factor. We consider the two functions defined as

$$f_1(\mathbf{r}) = \left(\frac{m}{2\pi}\right)^{1/2} \frac{e^{-mr}}{r} \quad (\text{A.1})$$

with $m = p_0/\sqrt{6}$, and

$$f_2(\mathbf{r}) = \left(\frac{\lambda^3}{\pi}\right)^{1/2} e^{-\lambda r} \quad (\text{A.2})$$

with $\lambda = p_0$ as different forms of the transition form factor. The Gaussian form defined in Eq. (29) corresponds to

$$f(\mathbf{r}) = \left(\frac{p_0^2}{2\pi}\right)^{3/4} \exp\left[-\frac{p_0^2 r^2}{4}\right], \quad (\text{A.3})$$

in the coordinate space. The parameters m and λ are fixed to reproduce the same ‘root mean square radius’

$\left(\int |f|^2 r^2 d\mathbf{r}\right)^{1/2}$ with the Gaussian form factor.

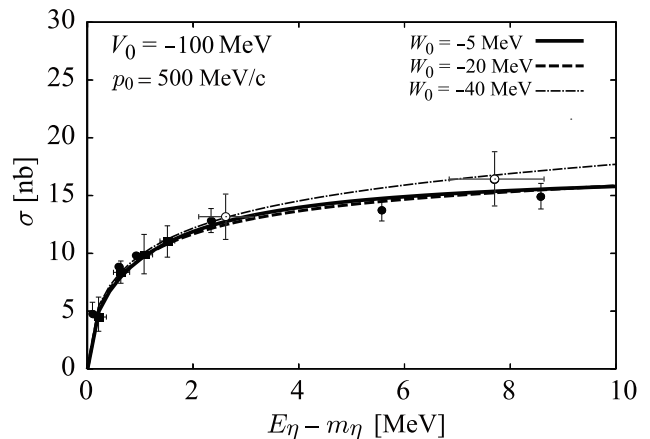


Fig. A.1. Same as Fig. 9 except for the transition form factor $f_1(\mathbf{r})$ defined in Eq. (A.1) is used instead of that in Eqs. (29) and (A.3).

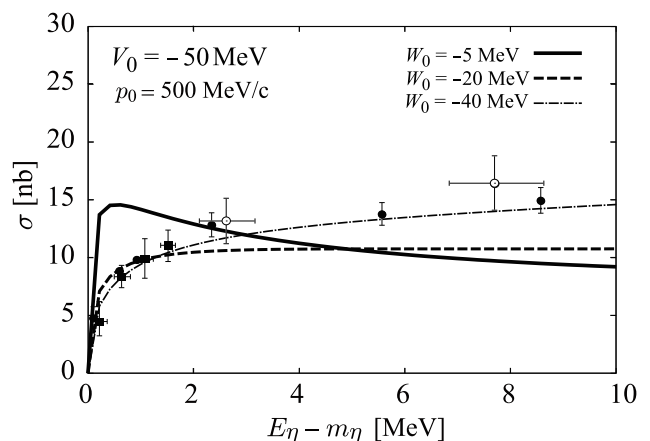


Fig. A.2. Same as Fig. 11 except for the transition form factor $f_1(\mathbf{r})$ defined in Eq. (A.1) is used instead of that in Eqs. (29) and (A.3).

We show the calculated results with $f_1(\mathbf{r})$ in Figs. A.1–A.4 and results with $f_2(\mathbf{r})$ in Figs. A.5–A.8, which correspond to Figs. 9, 11, 17, 19 obtained with $f(\mathbf{r})$ with $p_0 = 500$ MeV/c. These results are observables which can be compared with the appropriate experimental data. We have found that all results resemble each other and that the numerical results are robust to the choice of the functional form of the transition form factor.

References

1. Q. Haider and L. C. Liu, Phys. Lett. B **172**, (1986) 257; Phys. Rev. C **34**, (1986) 1845.
2. R. E. Chrien *et al.*, Phys. Rev. Lett. **60**, (1988) 2595.
3. J. Berger *et al.*, Phys. Rev. Lett. **61**, (1988) 919.
4. M. Kohno and H. Tanabe, Phys. Lett. B **231**, (1989) 219.
5. M. Kohno and H. Tanabe, Nucl. Phys. A **519**, (1990) 755.
6. H. C. Chiang, E. Oset and L. C. Liu, Phys. Rev. C **44**, (1991) 738.

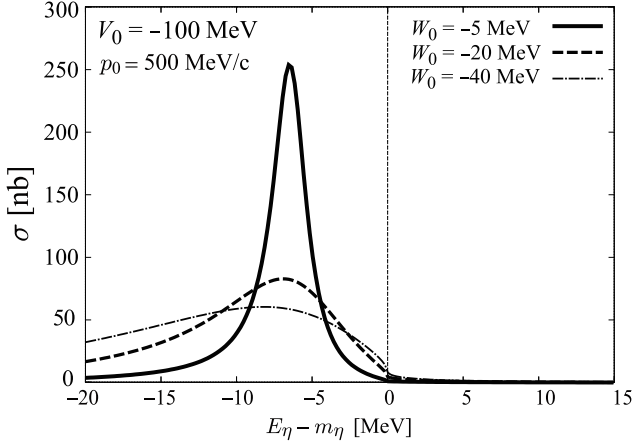


Fig. A.3. Same as Fig. 17 except for the transition form factor $f_1(\mathbf{r})$ defined in Eq. (A.1) is used instead of that in Eqs. (29) and (A.3).

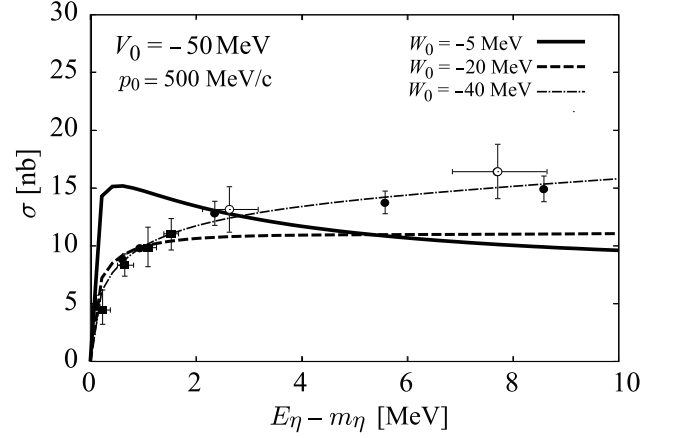


Fig. A.6. Same as Fig. 11 except for the transition form factor $f_2(\mathbf{r})$ defined in Eq. (A.2) is used instead of that in Eqs. (29) and (A.3).

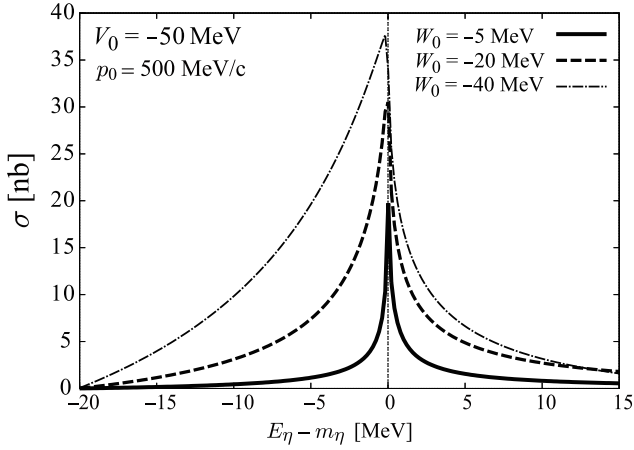


Fig. A.4. Same as Fig. 19 except for the transition form factor $f_1(\mathbf{r})$ defined in Eq. (A.1) is used instead of that in Eqs. (29) and (A.3).

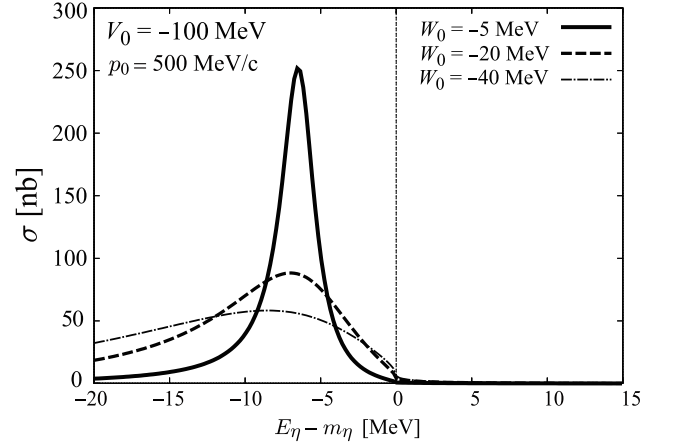


Fig. A.7. Same as Fig. 17 except for the transition form factor $f_2(\mathbf{r})$ defined in Eq. (A.2) is used instead of that in Eqs. (29) and (A.3).

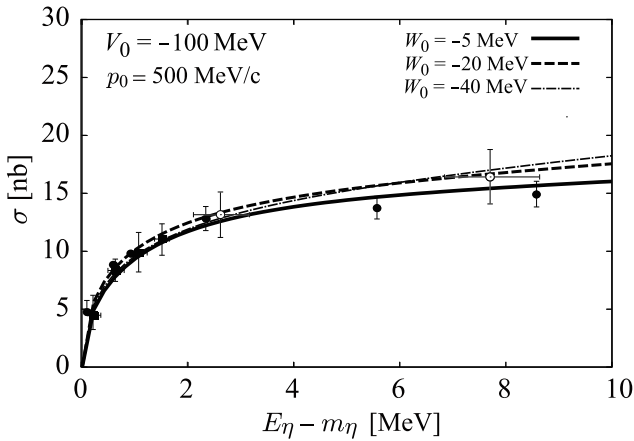


Fig. A.5. Same as Fig. 9 except for the transition form factor $f_2(\mathbf{r})$ defined in Eq. (A.2) is used instead of that in Eqs. (29) and (A.3).

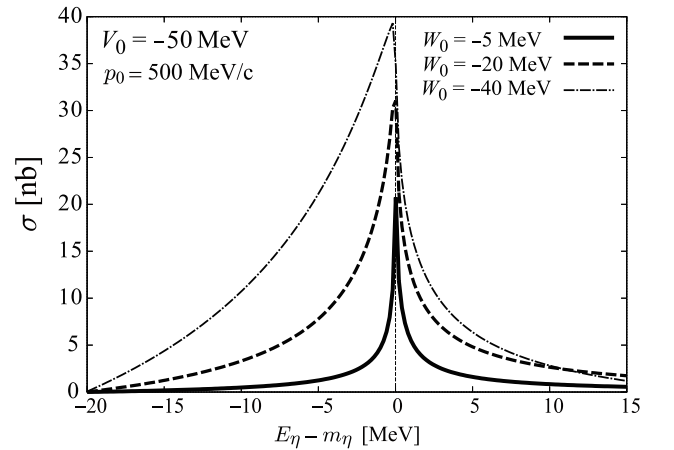


Fig. A.8. Same as Fig. 19 except for the transition form factor $f_2(\mathbf{r})$ defined in Eq. (A.2) is used instead of that in Eqs. (29) and (A.3).

7. G. A. Sokol and V. A. Tryasuchev, Bull. Lebedev Phys. Inst. **1991N4**, 21 (1991) [Kratk. Soobshch. Fiz. 4, 23 (1991\SPLRD, 4, 2124. 1991)]; G. A. Sokol, T. A. Aibergenov, A. V. Kravtsov, A. I. L'vov, and L. N. Pavlyuchenko, Fizika B **8**, 85 (1999).
8. J. D. Johnson *et al.*, Phys. Rev. C **47**, (1993) 2571.
9. T. Waas and W. Weise, Nucl. Phys. A **625**, (1997) 287.
10. K. Tsushima, D. H. Lu, A. W. Thomas and K. Saito, Phys. Lett. B **443**, (1998) 26; K. Saito, K. Tsushima, D. H. Lu and A. W. Thomas, Phys. Rev. C **59**, (1999) 1203.
11. R. S. Hayano, S. Hirenzaki and A. Gillitzer, Eur. Phys. J. A **6**, (1999) 99.
12. T. Inoue and E. Oset, Nucl. Phys. A **710**, (2002) 354.
13. C. Garcia-Recio, J. Nieves, T. Inoue and E. Oset, Phys. Lett. B **550**, (2002) 47.
14. D. Jido, H. Nagahiro and S. Hirenzaki, Phys. Rev. C **66** (2002) 045202; Nucl. Phys. A **721**, (2003) 665.
15. H. Nagahiro, D. Jido and S. Hirenzaki, Phys. Rev. C **68**, (2003) 035205.
16. M. Pfeiffer *et al.*, Phys. Rev. Lett. **92**, (2004) 252001.
17. C. Hanhart, Phys. Rev. Lett. **94**, (2005) 049101.
18. H. Nagahiro, D. Jido and S. Hirenzaki, Nucl. Phys. A **761**, (2005) 92.
19. N. G. Kelkar, K. P. Khemchandani and B. K. Jain, J. Phys. G **32**, (2006) L19.
20. D. Jido, E. E. Kolomeitsev, H. Nagahiro and S. Hirenzaki, Nucl. Phys. A **811**, (2008) 158.
21. C. Y. Song, X. H. Zhong, L. Li and P. Z. Ning, Europhys. Lett. **81**, (2008) 42002.
22. A. Budzanowski *et al.* [COSY-GEM Collaboration], Phys. Rev. C **79**, (2009) 012201; V. Jha *et al.* [GEM Collaboration], Int. J. Mod. Phys. A **22**, (2007) 596.
23. H. Nagahiro, D. Jido and S. Hirenzaki, Phys. Rev. C **80**, (2009) 025205.
24. Q. Haider and L. C. (L. C.) Liu, Int. J. Mod. Phys. E **24** 10, (2015) 1530009.
25. K. P. Khemchandani, N. G. Kelkar and B. K. Jain, Nucl. Phys. A **708** (2002) 312.
26. K. P. Khemchandani, N. G. Kelkar and B. K. Jain, Phys. Rev. C **68** (2003) 064610.
27. K. P. Khemchandani, N. G. Kelkar and B. K. Jain, Phys. Rev. C **76** (2007) 069801.
28. J. J. Xie, W. H. Liang, E. Oset, P. Moskal, M. Skurzok and C. Wilkin, Phys. Rev. C **95** (2017) no.1, 015202.
29. W. Krzemien, P. Moskal and M. Skurzok, Acta Phys. Polon. B **46**, (2015) 757.
30. W. Krzemien, P. Moskal and M. Skurzok, Few Body Syst. **55**, (2014) 795.
31. W. Krzemien *et al.* [WASA-at-COSY Collaboration], Acta Phys. Polon. B **45**, (2014) 689.
32. P. Adlarson *et al.* [WASA-at-COSY Collaboration], Phys. Rev. C **87**, (2013) 035204.
33. M. Skurzok *et al.* [WASA-at-COSY Collaboration], Acta Phys. Polon. B **47**, (2016) 503.
34. M. Skurzok, P. Moskal and W. Krzemien, Prog. Part. Nucl. Phys. **67**, (2012) 445.
35. P. Adlarson *et al.*, Nucl. Phys. A **959** (2017) 102.
36. N. G. Kelkar, Eur. Phys. J. A **52** (2016) no.10, 309.
37. R. Frascaria *et al.*, Phys. Rev. C **50**, (1994) 537.
38. N. Willis *et al.*, Phys. Lett. B **406**, (1997) 14.
39. A. Wronska *et al.*, Eur. Phys. J. A **26**, (2005) 421.
40. O. Morimatsu and K. Yazaki, Nucl. Phys. A **435**, (1985) 727; A **483**, (1988) 493.
41. R. S. Bhalerao and L. C. Liu, Phys. Rev. Lett. **54** (1985) 865.
42. S. A. Rakityansky, S. A. Sofianos, M. Braun, V. B. Belyaev and W. Sandhas, Phys. Rev. C **53** (1996) R2043. doi:10.1103/PhysRevC.53.R2043
43. N. G. Kelkar, Phys. Rev. Lett. **99** (2007) 210403 doi:10.1103/PhysRevLett.99.210403 [arXiv:0711.4066 [quant-ph]].
44. A. Fix and O. Kolesnikov, Phys. Lett. B **772** (2017) 663.
45. J. Kulpa and S. Wycech, Acta Phys. Polon. B **29** (1998) 3077.
46. A. Cieplý and J. Smejkal, Nucl. Phys. A **919** (2013) 46.
47. A. Cieplý, E. Friedman, A. Gal and J. Mare, Nucl. Phys. A **925** (2014) 126.